Journal of Ocean Engineering and Science 10 (2025) 492–508

Contents lists available at ScienceDirect

Journal of Ocean Engineering and Science

journal homepage: www.elsevier.com/locate/joes

Research Paper

Design and comparative analysis of mooring systems for a combined wind and wave energy system at intermediate water depth

Chern Fong Lee, Sindre Fjermedal, Muk Chen Ong*

Department of Mechanical and Structural Engineering and Materials Science, University of Stavanger, 4036 Stavanger, Norway

ARTICLE INFO

Article history:
Received 24 June 2024
Revised 18 September 2024
Accepted 21 November 2024
Available online 11 January 2025

Keywords:
Floating offshore wind turbine
Combined wind and wave energy device
Mooring system
Intermediate waters
Synthetic fibre rope
Polyester rope

ABSTRACT

For intermediate water depths (typically ranging from 50 m to 80 m), designing steel catenary mooring systems for floating marine renewable energy (FMRE) platforms can be challenging due to the limited weight of suspended mooring lines. This can substantially increase mooring line tensions following large platform offsets. In contrast, mooring systems using synthetic fibre ropes offer the potential to prevent large platform offsets while reducing peak mooring line tensions. In this study, novel semi-taut mooring systems incorporating polyester ropes and steel chains are proposed for a combined wind and wave energy system – the semi-submersible flap torus combination (STFC) concept, deployed at a 50 m water depth. The STFC integrates a semi-submersible floating offshore wind turbine (FOWT), a torus wave energy converter (WEC) and three flap-type WECs. The dynamic responses of the STFC with different semi-taut mooring configurations under operational and survival environmental conditions are assessed in terms of key performance parameters such as the platform's motion responses and mooring line tensions. These performance parameters are compared against those of a chain-catenary mooring system. With the use of semi-taut mooring systems, significantly smaller mooring footprints as compared to the chain-catenary mooring systems can be achieved. Moreover, it is demonstrated that the semi-taut mooring systems are effective in reducing the maximum tension of the mooring lines. A basic cost analysis further indicates that semi-taut mooring systems offer substantial cost advantages over chain-catenary moorings in intermediate water depths.

1. Introduction

Renewable energy is on track to become the leading source of global electricity by 2025, overtaking coal as the primary source of electricity. The growth is partly driven by a forecasted doubling of wind energy capacity by 2027, with offshore wind capacity accounting for 20 % of this growth [1]. Within the offshore wind industry, a considerable share of the market comprises floating offshore wind turbines (FOWTs), which by 2050 are set to account for 15 % of the offshore wind capacity [2]. As the offshore wind industry experiences rapid growth, wave energy, though not in the spotlight, is still anticipated to play a role in the global shift toward renewable energy sources. Nonetheless, the full commercialization of wave energy faces several challenges, with a significant obstacle being a higher levelized cost of energy (LCOE) as compared to other renewable energy sources [3].

Depending on the depth and seabed condition, different concepts of foundations are utilized for the construction of offshore wind farms. At shallow water depths, typically between 30 - 50 m, bottom-fixed foundations such as the monopiles are the most common. For the water depths in the region of 100 m and beyond, floating foundations such as spars, semi-submersibles and tension-leg platforms (TLPs) emerge as sensible candidates due to the increased cost and complexity that is associated with bottom-fixed solutions. However, for intermediate water depths ranging from 50 to 80 m, there exists no definitive consensus regarding the choice of platform. In these water depths, the question of "floating or bottom-fixed?" must be addressed with a focus on economic viability.

At intermediate water depths, more expensive jacket structures are viable options but face significant cost increments as the depth increases. Alternatively, semi-submersible platforms can be used due to their characteristic shallow draft. However, the utilization of floating foundations at intermediate water depths introduces a distinct set of challenges, one of which is the design of mooring systems. With a reduced water column, it is

* Corresponding author.
E-mail address: muk.c.ong@uis.no (M.C. Ong).

https://doi.org/10.1016/j.joes.2024.11.002

Nomenclature

A	Mooring rope cross-sectional area
E	Young's Modulus
H_s	Significant wave height
h	Water depth
I	Turbulence intensity
k_G	Catenary mooring line horizontal restoring stiffness
k_E	Taut synthetic fibre rope mooring line horizontal restoring stiffness
l	Mooring line length
L_i	Synthetic fibre rope unstretched length
L_0	Synthetic fibre rope stress-free length
m_i	Synthetic fibre rope unstretched mass per unit length
m_0	Synthetic fibre rope stress-free mass per unit length
r	Structure nodal displacement
$\dot{r}$	Structure nodal velocity
$\ddot{r}$	Structure nodal acceleration
R^I	Inertia force vector
R^D	Damping force vector
R^S	Internal structural reaction force vector
R^E	External force vector
$\bar{T}_{max}$	Synthetic fibre rope maximum mean tension
$\bar{T}$	Synthetic fibre rope mean tension
T_{pre}	Mooring line pre-tension
T_p	Wave peak period
T_H	Horizontal mooring line tension
$\bar{U}$	Mean wind speed measured at hub height
U_c	Current speed
w	Mooring line mass per unit length
θ	Mooring line departure angle
ε	Synthetic fibre rope strain
ε_0	Synthetic fibre rope stress-free strain
ε_m	Synthetic fibre rope mean strain

challenging for conventional catenary mooring configurations to maintain their geometries, and this results in highly nonlinear mooring stiffness characteristics. Xu et al. [4] discovered that by using clump weights, the mooring stiffness characteristics can be improved. The nonlinearity of mooring restoring stiffness can also be mitigated by using synthetic fibre ropes in taut configurations since they are less influenced by the water depth and more reliant on the material stiffness, in contrast to the conventional catenary mooring configurations.

Since its introduction by Petrobras in 1997, synthetic fibre ropes have been used as cost-effective and reliable mooring materials in the oil and gas sector [5]. Weller et al. [6] proposed that FOWTs and WECs will benefit from compliant mooring materials such as polyester or nylon as they offer superior fatigue and load-reducing properties as compared to conventional chain mooring systems. In 2018, BW IDEOL launched the Floatgen FOWT demonstrator off the coast of Le Croisic [7], making it one of the world's firsts in using nylon lines for the permanent mooring system.

Despite the apparent weight and cost benefits associated with the use of synthetic fibre mooring lines, a thorough understanding and accurate modelling of the material properties are required to estimate its influence on the dynamics of FOWTs. DNV [8] recommends a modelling method based on the Syrope Joint Industrial Program (JIP) [9]. According to this method, the quasi-static stiffnesses of the mooring lines are used to estimate mean loads and platform offsets, while the dynamic stiffnesses are applied to estimate the dynamic loads and platform motions. Recent studies by Xu et al. [4] and Sørum et al. [10,11] demonstrated the applicability of the Syrope model and its capability to accurately predict the dynamic behaviour of polyester and nylon mooring ropes used for FOWTs. Additionally, as shown by Xu et al. (2022), the use of synthetic fibre ropes has the potential to reduce the cost of mooring.

Both FOWTs and WECs have traditionally been installed as individual devices. However, the statistically correlated nature of wind and waves presents an opportunity to combine a FOWT and multiple WECs into an integrated device. This allows for the co-sharing of supporting structures, power cables, mooring systems, and marine space, which is expected to reduce the LCOE [12]. For example, the costs of mooring systems for FOWTs and WECs account for 40 % and 30 % of CAPEX, respectively [2,13]. To date, several combined wind and wave energy concepts such as Flex2power [14], Poseidon Wave and Wind [15], W2Power [16] and the semi-submersible torus flap combination (STFC) [17] are in development. Despite recent technological advancements, combined wind and wave energy devices continue to grapple with challenges which include complicated dynamic behaviour and limited power extraction from the WECs [15]. Hence, it is crucial to continue driving down the development costs to render them economically feasible.

In this study, different mooring systems for the STFC deployed at an intermediate water depth of 50 m are investigated. In addressing the challenges posed by pure catenary and pure taut mooring systems, semi-taut mooring systems consisting of top chain segments, intermediate polyester rope segments and bottom chain segments are proposed. The dynamic behaviour of the floater and mooring lines are simulated under aligned wind and wave environmental conditions in a fully coupled manner. The performance of all mooring systems is compared in terms of the moored platform's horizontal offsets, motion characteristics and mooring line tensions. Lastly, a cost analysis and design recommendations for the STFC's mooring systems at intermediate water depths are given.

2. Description of concept

2.1. Semi-submersible torus flap combination (STFC)

The STFC concept proposed by Lee et al. [17] is an integrated wind and wave energy concept that combines a floating horizontal axis wind turbine (FHAWT), three flap-type wave energy converters (WECs), and a torus WEC. The supporting platform is a steel semi-submersible, 5-MW-CSC (CSC) developed by Luan et al. [18] to support the 5-MW NREL wind turbine [19]. The station-keeping of the supporting platform is achieved through three catenary wire rope mooring lines attached to the side columns. The graphical representations of CSC and the STFC concept are shown in Fig. 1. The properties are provided in Table 1.

The flap-type WECs, each comprising an elliptic-cylindrical buoy with two supporting arms are hinged to the top of the pontoon. The torus WEC is installed through the central column of the platform and constrained to move only in the heave direction. During operations, the wave-induced motions of the WECs are converted into kinetic energy, and the energy is absorbed by the power take-off (PTO) systems. The PTO mechanisms of the flap type and the torus WECs are illustrated in Fig. 2. The PTO system connecting the torus and the hull consists of hydraulic cylinders, a hydraulic motor, accumulators, and a generator, which generates electricity from the heaving motion of the torus induced by ocean waves.

To avoid excessive structural loads, the WECs are taken out of service and put into survival modes in extreme sea states. The present study defines the survival environmental conditions as sea states with H_s beyond 6 m. In the survival mode, the flap-type WECs are locked in their neutral (upright) positions. As the torus contributes >66 % of the total water plane area, the supporting

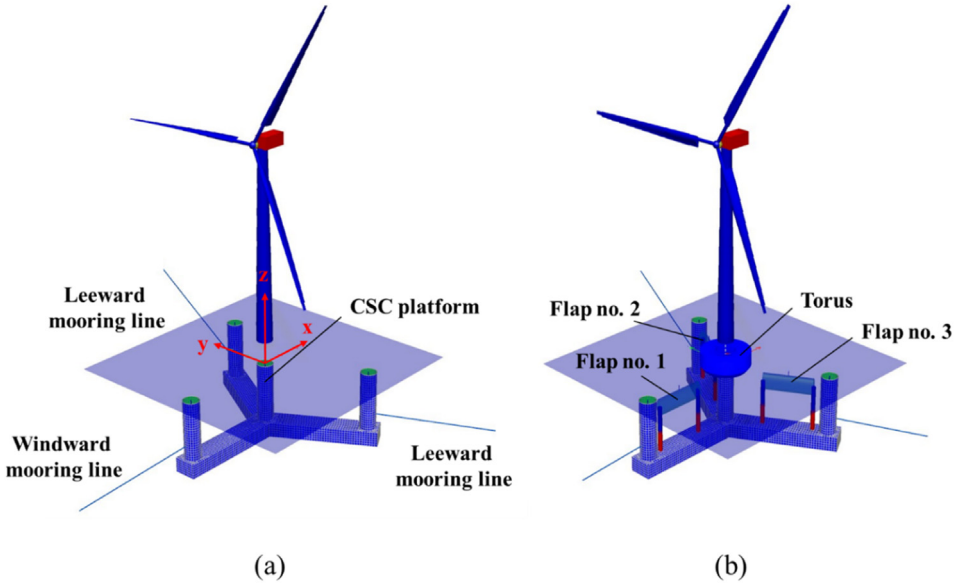

Fig. 1. Graphical illustration of the (a) CSC and (b) STFC concepts.

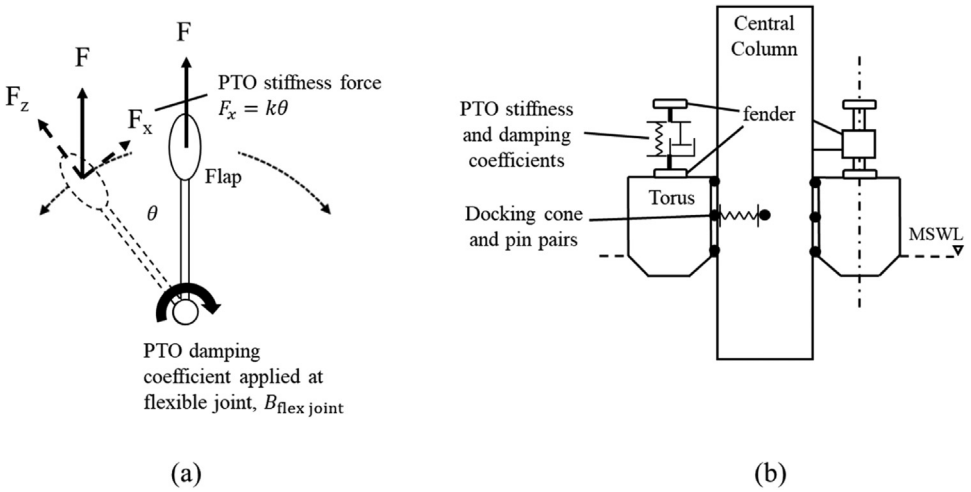

Fig. 2. Mechanism of a flap type WEC and a torus WEC.

platform is ballasted to the point that the torus is fully submerged. With the help of the PTO hydraulic cylinders, the torus is further lowered and locked at full stroke such that its top plate is 3 m below the mean sea water level in the survival mode. It is calculated that another 3964 tonnes of ballast water are required to achieve this level of platform draft in the survival mode. An illustration comparing the operational and survival modes of STFC is shown in Fig. 3. In the parking positions of the WECs, it is assumed that the loadings due to slamming and green water, specifically concerning the torus WEC will have negligible influence on the supporting platform due to the huge difference in inertia properties. Further investigations into the local loadings on the connection points during extreme environmental conditions will be included in a follow-up study.

3. Numerical model

Fully coupled numerical modelling of CSC and STFC and the mooring systems are established using SIMA [20,21], a dynamic simulation software developed by SINTEF Ocean.

3.1. CSC and STFC

The wind turbine hub and nacelle, semi-submersible, and the buoys for the torus and flap type WECs are modelled as rigid bodies with concentrated masses. For the submerged bodies, hydrodynamic added mass, potential damping coefficients and first-order wave excitation loads are determined through frequency domain hydrodynamic analysis using WADAM [22]. Viscous loads on the submerged rigid bodies are calculated as Morison drag forces (Morison et al., 1950). Difference frequency wave loads are only considered for the semi-submersible through the implementation of full quadratic transfer function (QTF).

The wind turbine blades, tower and supporting arms for the flap-type WECs are modelled as distributed mass beam elements while the mooring lines are modelled as bar elements. The buoys and clump weights are modelled as points with concentrated masses and prescribed volumes. Morison's equation (Morison et al., 1950) is used to determine hydrodynamic loads on the supporting arms of the flap-type WECs and the mooring lines. The generator shaft of the wind turbine is composed of a non-rotating and a rotating component separated by a flexible joint. Generator torque is

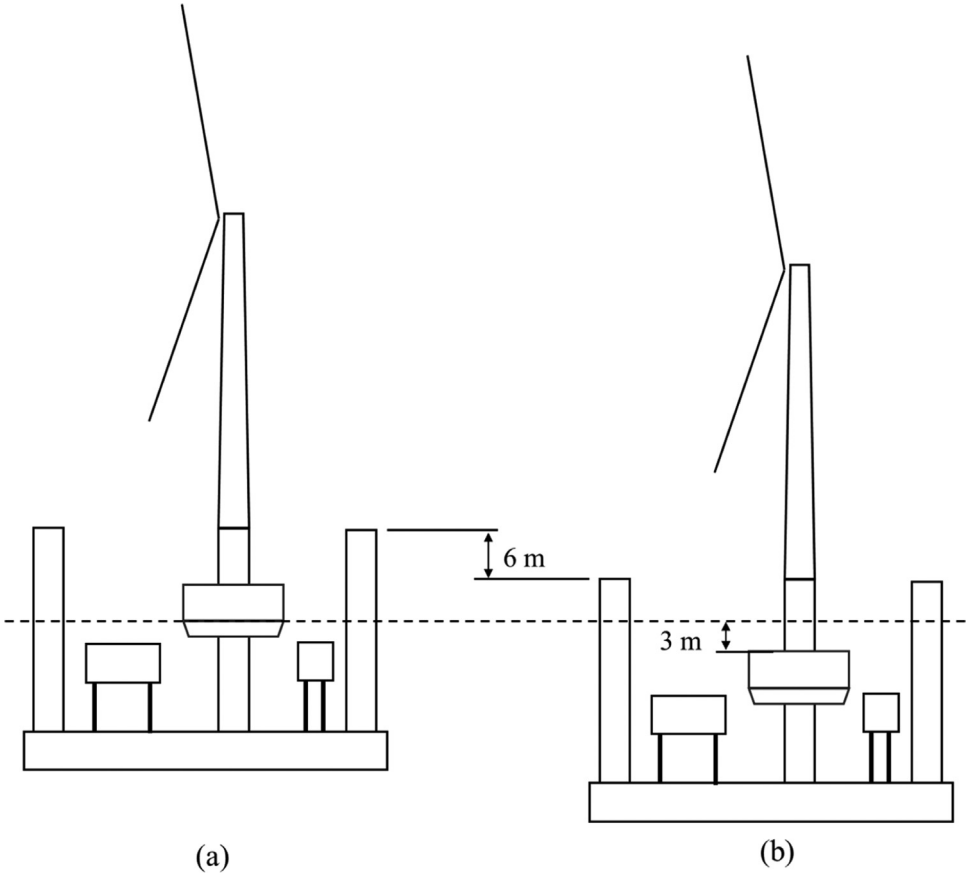

Fig. 3. (a) Operational and (b) survival modes of STFC.

Table 1
Main properties of STFC.

Property	Unit	Value
CSC semi-submersible		
Draft	m	30
Displacement	tonnes	10 500
Operational water depth	m	200
Single mooring line		
Mass per unit length	kg/m	115
Unstretched mooring line length	m	1073
Clump weight in water	tonnes	15
Distance of clump weight from the fairlead	m	240
Flap type WEC		
Dimension of an elliptic cylinder (length×width×height)	m	20×7 × 3.5
Displacement	tonne	394
Mass	kg	100
Length of one supporting arm	m	18.5
Mass of one supporting arm	kg	33.08
Displacement of one support arm	tonne	33.5
Torus WEC		
Outer diameter of the torus	m	20
Inner diameter of the torus	m	8
Draft	m	2
Displacement	tonnes	423.7

applied on the flexible joint in accordance with the control strategy described by Jonkman et al. [19]. The PTO of the flap-type WECs are modelled at the hinge connections as linear rotational dampers while the PTO of the torus WEC is modelled as a linear spring-dashpot.

Fully coupled time-domain simulations are performed using SIMA [20,21], which solves for the structural dynamic equations in time-domain given by,

$$R^I(r,\ddot{r},t) + R^D\left(r,\dot{r},t\right) + R^S(r,t) = R^E\left(r,\dot{r},t\right) \quad (1)$$

where t is time, R^I is the inertia force vector, R^D is the damping force vector, R^S is the internal structural reaction force vector, and R^E is the external force vector. r, r, r are the structural displacement, velocity, and acceleration vectors, respectively.

3.2. Modelling of polyester ropes

The Syrope model proposed by Falkenberg et al. [9] is used in this study to model the stiffness characteristics of the polyester ropes. The model is built on the assumption that a synthetic fibre rope can be represented using the spring-dashpot model shown in Fig. 4 by Flory et al. [23]. The spring-dashpot model can be further simplified by assuming that the installation of the synthetic fibre rope happens at a tension above the expected maximum tension during its lifetime. This installation procedure prevents any further permanent stretching of the synthetic fibre rope after installation [24]. Moreover, in comparison to the instantaneous elastic strain, the visco-elastic strain is a slow process. Hence, a synthetic fibre rope can be represented as a spring with tension-dependent stiffness values post-installation.

The Syrope model can be described using four curves: original curve, original working curve, working curve and dynamic stiffness [9]. The original curve represents a new synthetic fibre rope subject to rapid loading in the initial bedding-in process. The original working curve is generated when the synthetic fibre rope is subjected to loading at the historically maximum mean tension,

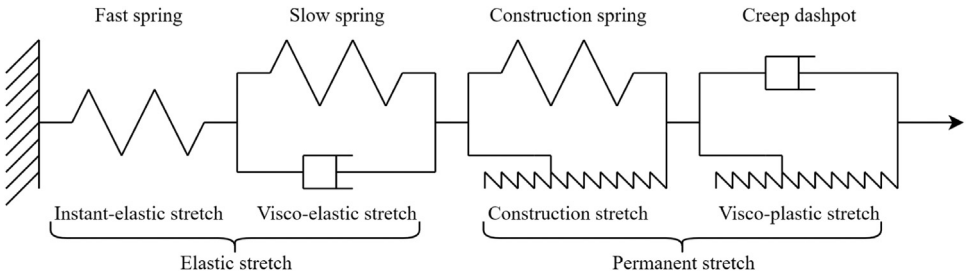

Fig. 4. Spring-dashpot model of a synthetic fibre rope.

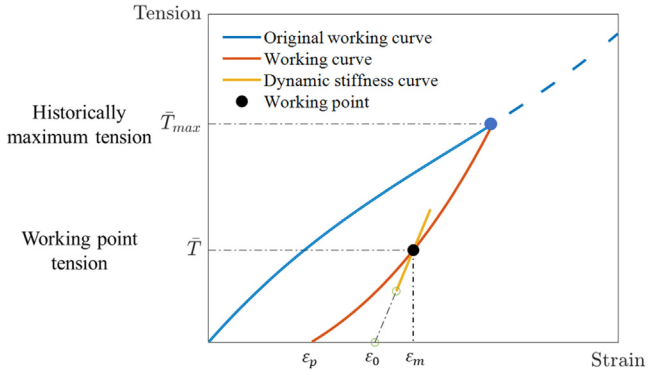

Fig. 5. The Syrope model.

$\bar{T}_{max}$, which introduces additional permanent strain, ε_p that must be taken into account in the working curve. For any tension value below $\bar{T}_{max}$, the tension-strain relationship will follow the working curve. The slope of the working curve at the corresponding working point represents the static stiffness. The dynamic stiffness is proposed to be linearly dependent on the mean tension. The Syrope model without the original curve is presented in Fig. 5.

In practice, Syrope is implemented using tension-strain test data from sub-rope testing. In the present study, a simplified Syrope model is employed due to the scarcity of available test data. The simplified model assumes that tension in the mooring lines during operation is lower than the installation tension. Therefore, no further permanent and visco-elastic strain of the synthetic fibre rope is expected. Hence only one working curve is considered. As shown in Fig. 5, the static stiffness is observed to be nonlinear. However, in this study, static stiffness that is linearly dependent on mean tension, $\bar{T}$ and minimum breaking strength (MBS) is assumed. The expression of the linearised static stiffness can be given by,

$$EA_s = \frac{d\bar{T}}{d\varepsilon} = a \cdot \bar{T} + b \cdot \text{MBS} \tag{2}$$

where ε is the strain of the rope while a and b are constants estimated from test data. The dynamic stiffness can too be assumed to be a linear function of $\bar{T}$ and MBS given by,

$$EA_d = \frac{d\bar{T}}{d\varepsilon} = c \cdot \bar{T} + d \cdot \text{MBS} \tag{3}$$

where c and d are constants obtained from the dynamic testing of ropes. In this study, the values of constants a, b, c and d are provided in Section 5.3. Fig. 6 shows the implementation workflow of taut and semi-taut mooring system analyses in the present study. It is described in detail as follows:

- **Step 1**: Initialize the mooring system with anchor radius, unstretched line length, pre-tension T_{pre}, MBS and stiffness constants a, b, c and d. Without applying environmental loads, calculate the static stiffness., EA_s via Eq. (2). The final anchor radius is determined when the required pre-tension T_1 is achieved with its corresponding static stiffness.
- **Step 2**: For each environmental condition (EC), static analysis is carried out using the mean environmental loads to determine the mean tension. The mean tension is used to calculate the updated EA_s value according to Eq. (2). Repeat Step 2 and update EA_s until the $\bar{T}$ value on each mooring line converges.
- **Step 3**: Using $\bar{T}$ obtained from Step 2, calculate EA_d based on Eq. (3). As shown in Fig. 5, the stress-free strain used in the dynamic analysis, ε_0 can be estimated using EA_d given by,

$$\varepsilon_0 = \varepsilon_m - \bar{T}/EA_d \tag{4}$$

where ε_m is the mean strain obtained in the static analysis (Step 2). Update the unstretched line length by including ε_0. The stress-free length can be calculated as,

$$L_0 = L_i + \varepsilon_0 L_i \tag{5}$$

and the updated mass distribution can be calculated as,

$$m_0 = m_i \frac{L_i}{L_0} \tag{6}$$

where L_i and m_i are the initial unstretched length and mass per unit length, respectively.

- **Step 4**: Perform dynamic analysis using EA_d. As a sanity check, the mean tensions calculated from Step 4 (dynamic) and Step 2 (static) should be equal.

4. Environmental conditions

Irregular wave conditions are described by significant wave heights, H_s, and peak periods, T_p, according to the Jonswap spectrum. Turbulent wind conditions are generated using the software Turbsim [25], specified by mean wind speed at hub height, $\bar{U}$, and turbulence intensity, I. Aligned wind and wave loadings are assumed. The dynamic responses of STFC in operation are evaluated using six operational ECs based on the data from an offshore site in the northern North Sea [26]. For the survival conditions of STFC, Design Load Case (DLC) 6.1 as defined in the IEC 61,400–3–1 standard [27] is considered in which the turbine is parked and the WECs are locked in an extreme sea state (ESS). The ESS is taken as the sea state with a 50-year return period. A surface current speed of 1 m/s is chosen, with a linearly decreasing current speed with depth given by,

$$U_c(z) = 1.0 \times \left(\frac{50+z}{50}\right) \text{ for } -50 \le z \le 0 \tag{7}$$

The total seven environmental load cases covering the operational and survival domain of CSC and STFC are used as shown in Table 2. For each EC, 6 random simulations are carried out to account for the statistical variation.

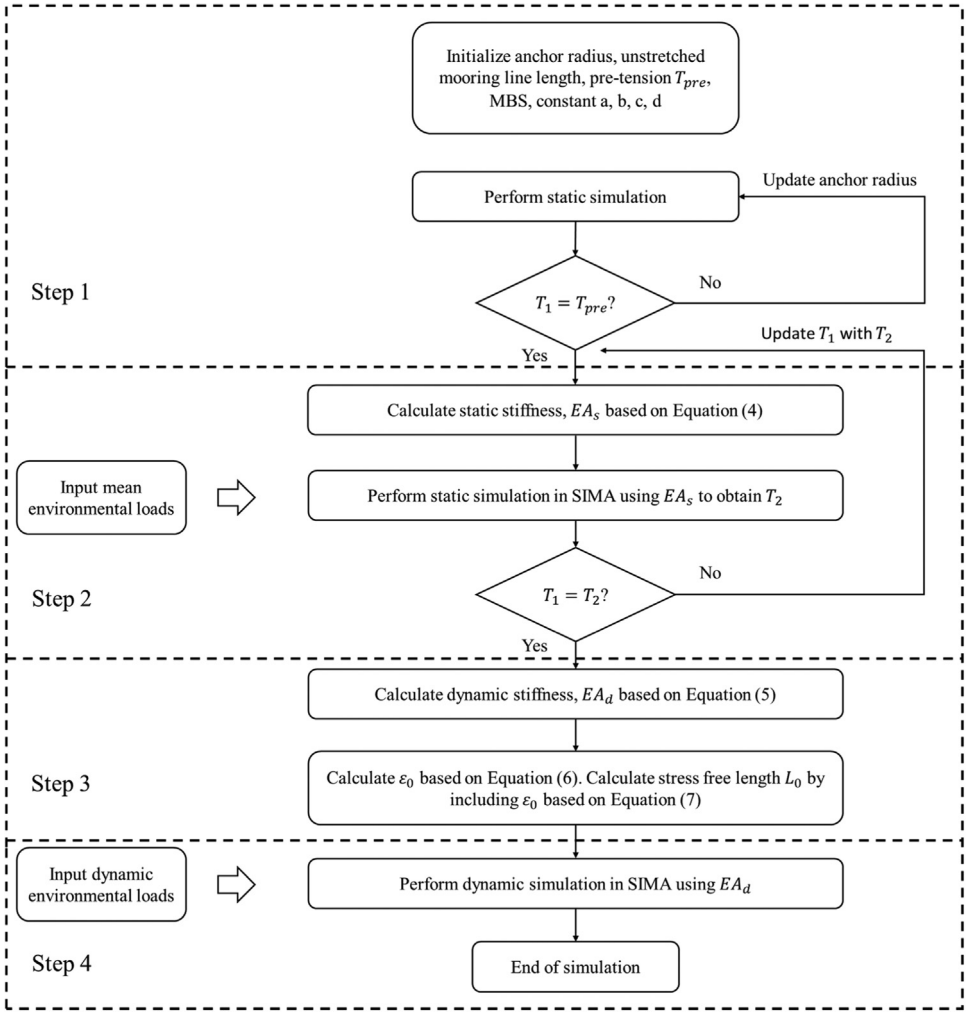

Fig. 6. Procedure for implementing the Syrope model.

Table 2
Environmental conditions.

Condition	$\bar{U}$ (m/s)	I (-)	H_s (m)	T_p (s)	U_c (m/s)	Seeds (-)	Duration (hour)
EC1	5	0.224	2.10	9.74	–	6	1
EC2	10	0.157	2.88	9.98	–	6	1
EC3	14	0.138	3.62	10.29	–	6	1
EC4	18	0.127	4.44	10.66	–	6	1
EC5	22	0.121	5.32	11.06	–	6	1
EC6	25	0.117	6.02	11.38	–	6	1
DLC 6.1	51.43	0.099	13.28	14.29	1	6	1

5. The design of mooring systems

5.1. Characteristics of mooring systems at intermediate water depths

The current state-of-the-art indicates that research on mooring designs for intermediate water depths predominantly concentrates on catenary mooring systems composed solely of chain links (Brommundt et al. [28], Benassai et al. [29], Pillai et al. [30]), a methodology that has long been validated in the oil and gas industry. For a chain catenary mooring system, its station-keeping capability is contributed by the chain weight, which generates the pre-tension required to keep the structure inplace. For an in-elastic chain, Faltinsen [31] demonstrated analytically that the horizontal restoring stiffness, k_G for a catenary mooring line can be expressed given by,

$$k_G = w\left[\frac{-2}{\left(1+2\frac{T_H}{wh}\right)^{\frac{1}{2}}} + \cosh^{-1}\left(1+\frac{wh}{T_H}\right)\right]^{-1} \tag{8}$$

where w is the unit weight of the mooring line, T_H is the horizontal mooring line tension and h is the water depth. This presents a challenge. With the water depth decreasing, the mooring line weight has to be increased to maintain the same level of pre-tension. Assuming that the mooring line weight is increased linearly with respect to the decreasing water depth, k_G increases with water depth as shown in Fig. 7. An increase in stiffness increases the natural frequencies of translational motions, shifting the resonance closer to wave frequencies.

Due to the limited water column, the rate of change in catenary shape is higher in shallower water depths. This directly leads to a higher rate of chain lift-off as the moored structure is displaced from its original position. As soon as the full length of the chain is lifted off, the restoring stiffness becomes purely elastic, and this results in a spike in tension. It is therefore common for the chain mooring systems in shallow water to have exceptionally long anchor radii if drag embedment anchors are to be used.

For taut mooring systems, synthetic fibre ropes are used instead of chains and steel wire ropes. As opposed to a catenary mooring system, the restoring stiffness of a taut mooring system is contributed mainly by the elastic stiffness. For a synthetic fibre moor-

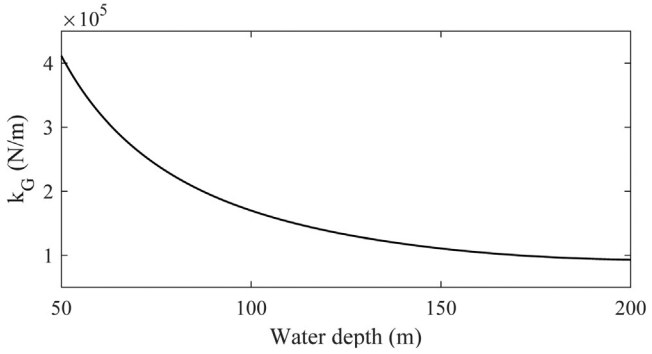

Fig. 7. Restoring stiffness of a catenary mooring line at different water depths.

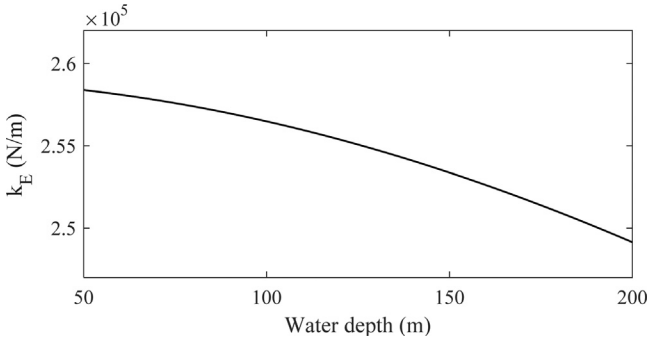

Fig. 8. Restoring stiffness of a taut mooring line in different water depths.

ing line of length l, its contribution to the elastic stiffness is given by,

$$k_E = \frac{EA\cos\theta}{l} \tag{9}$$

where E is the Young's modulus, A is the cross-sectional area and θ is the angle between the mooring line and the horizontal plane known as the departure angle. With the same anchor radius, the mooring line length has to be reduced to maintain the pre-tension as water depth reduces, which leads to an increase in k_E as shown in Fig. 8. By comparing Figs. 7 and 8, it can be observed that the restoring stiffness of the catenary more system increases more drastically than the taut mooring system as the water depth decreases.

5.2. Design Criteria for mooring systems at intermediate water depths

The mooring systems for STFC at intermediate water depths are evaluated in all design conditions in accordance with the following criteria:

1. The offset has to be limited to a reasonable range to avoid excessive damage on inter-array power cables.
2. Maximum tensions in the mooring lines should never exceed the MBS.
3. Loss of tension shall not occur in the mooring lines as this condition can potentially lead to large snap tension loads. This is connected to Criterion No 2.
4. The synthetic fibre ropes shall not be in contact with the seabed and floater to avoid abrasion of the synthetic fibres [8].

5.3. Mooring adaptations for intermediate waters

The original 3-line wire-rope-catenary mooring system of CSC and STFC designed for a water depth of 200 m is utilized as the

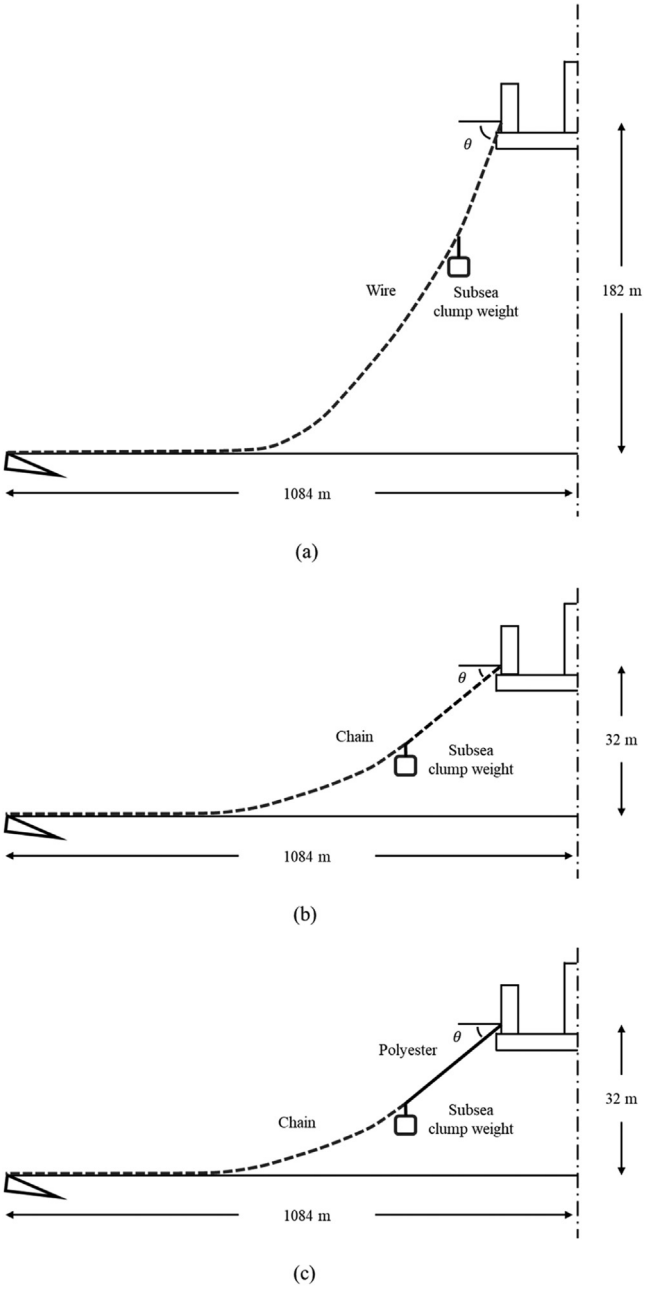

Fig. 9. (a) Baseline (b) 50 m chain catenary and (c) 50 m chain-and-polyester semi-taut mooring systems.

baseline for the design of mooring systems at intermediate waters. As illustrated in Fig. 1, one of the three mooring lines is oriented in the windward direction while the two remaining mooring lines are spaced 120° apart from the windward mooring line. For a water depth of 50 m, two different mooring configurations are introduced while retaining similar mooring line horizontal pretensions and mooring footprints as compared to the baseline configuration. These configurations can be categorized into – (1) the pure chain-catenary mooring configuration and (2) the semi-taut mooring configuration utilizing a combination of polyester ropes and chains as illustrated in Fig. 9. For the semi-taut mooring configuration, each mooring line consists of a top polyester rope segment and a bottom chain segment anchored to the seabed via a DEA. The length of the polyester rope is selected to be 40 m which is considerably shorter than the water depth. This constraint is to

Table 3
Mooring configurations.

System name	Horizontal pre-tension (kN)	Departure angle (°)	Water depth (m)	Anchor radius (m)	Top segment length (m)	Bottom segment length (m)	Clump weight (tonne)	Total line length (m)
baseline 200 m (1084 m)	1410	30.28	200	1084	240	833.0	15	1073.0
chain-50 m (1084 m)	1366	25.20	50	1084	40	1003.6	15	1043.6
semi-taut-50 m (1084 m)	1402	20.32	50	1084	40	992.9	15	1032.9

Table 4
Mooring line properties.

	Nominal diameter (m)	Mass in air (kg/m)	Submerged mass (kg/m)	Cross-sectional area (m^2)	Axial stiffness EA (kN)	MBS (kN)	a (-)	b (-)	c (-)	d (-)
Spiral rope	0.137	115.0	100.0	0.0147	3,080,000	16,769	–	–	–	–
Chain	0.130	370.0	321.8	0.0470	1,706,900	11,932	–	–	–	–
Polyester	0.203	26.5	6.8	0.0192	Eq. (4) & (5)	11,772	50	5.5	25	20

Table 5
Maximum 1-hour windward mooring line tension for the 200 m baseline, 50 m chain-catenary and 50 m chain-and-polyester semi-taut mooring configurations.

System name	Maximum tension (kN)	% MBS (%)
baseline 200 m (1084 m)	13,540	80.74
chain-50 m (1084 m)	15,670	131.33
semi-taut-50 m (1084 m)	14,510	123.26

prevent any touching down of polyester rope on the seabed. To compare the platform dynamic responses with different mooring systems in Fig. 9, the CSC FOWT without any WEC is first used as the subject for investigation. The polyester ropes in the semi-taut mooring configuration are selected based on the catalogue of BRIDON BEKAERT [32]. The chain specification is selected to have a similar MBS as compared to the polyester rope which leads to the selection of ORQ stud chain according to the catalogue of Ramnäs [33]. The properties of the mooring configurations in comparison are provided in Table 3 while the mooring line properties are shown in Table 4. The values of constants *a*, *b*, *c* and *d* in Table 4 are obtained from Tomren [34].

DLC 6.1 is selected for the evaluation of the design criteria as detailed in Section 5.2. Six randomly seeded 1-hour simulations under DLC 6.1 are carried out for the FOWT using different mooring configurations. In Table 5, the maximum 1-hour windward mooring line tensions in six random simulations are compared. It is observed that at 50 m water depth, the maximum windward mooring line tensions are 131 % and 123 % of the MBS for the chain-catenary and semi-taut configurations, respectively. Only a marginal reduction of peak tension with the use of a short polyester rope section, indicating that polyester rope with lengths much longer than the water depth could be required. Hence, the mooring configuration with the short polyester segment will not be further investigated.

For the 50 m chain-catenary system, the same simulations are carried out with increasing anchor radii while maintaining the same departure angle and pre-tension. The maximum 1-hour windward line tensions of the chain-catenary system at 50 m water depth with different anchor radii are shown in Fig. 10. As the anchor radius approaches 3000 m, the maximum windward mooring line tension reduces to 10,730 kN (90 % MBS). Any further increase in anchor radius past this point will only provide a marginal reduction in maximum tension.

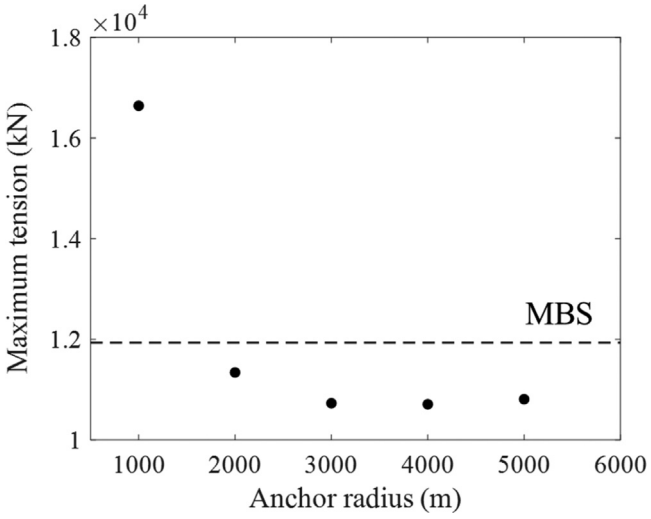

Fig. 10. Maximum tension of the windward mooring line for the chain-catenary system at 50 m water depth with different anchor radii.

5.4. Semi-taut variations

The strength of polyester ropes lies in their ability to generate restoring force through elastic straining. It is discovered in Section 5.3 that short polyester ropes result in tension responses similar to that of a pure catenary system. Hence, the polyester rope length must be increased considerably to achieve a more compliant mooring restoring characteristic. From Eq. (9), the axial stiffness of a line reduces with increasing length. If the horizontal pre-tension is to be maintained, this increase in rope length will be accompanied by a reduction in the departure angles. To reduce the risk of contact between the polyester ropes and the seabed, a subsea buoy is attached at the beginning of the bottom chain segment of each mooring line. The presence of the subsea buoys has a secondary function of further reducing the departure angle such that the mooring lines are more aligned in the translational (horizontal) direction. In this section, three semi-taut variations with different polyester rope lengths are proposed. For each semi-taut variation, the bottom chain segments are adjusted accordingly to achieve similar horizontal pre-tensions as compared to the baseline configurations. In addition to the effect of varying polyester rope and chain lengths, the effect of adding clump weights is in-

Table 6
Mooring configurations of the chain-catenary semi-taut variations at 50 m waters.

System name	Horizontal pre-tension (kN)	Departure angle (°)	Anchor radius (m)	Rope length (m)	Chain length (m)	Buoy (kN)	Clump weight (t)	Total line length (m)
chain-50 m (3000 m)	1366	25.20	3000	–	2958.0	–	15	2958.0
semitaut-V1	1428	3.34	1000	572.5	377.9	184	–	950.4
semitaut-V2	1427	3.71	1000	473.6	477.8	184	–	951.4
semitaut-V3	1426	4.17	1000	374.8	577.8	184	–	952.6
semitaut-V1clump	1417	7.70	1000	572.9	377.9	184	15	950.8
semitaut-V2clump	1416	7.99	1000	474.0	477.9	184	15	951.9
semitaut-V3clump	1415	8.21	1000	375.2	577.7	184	15	952.9

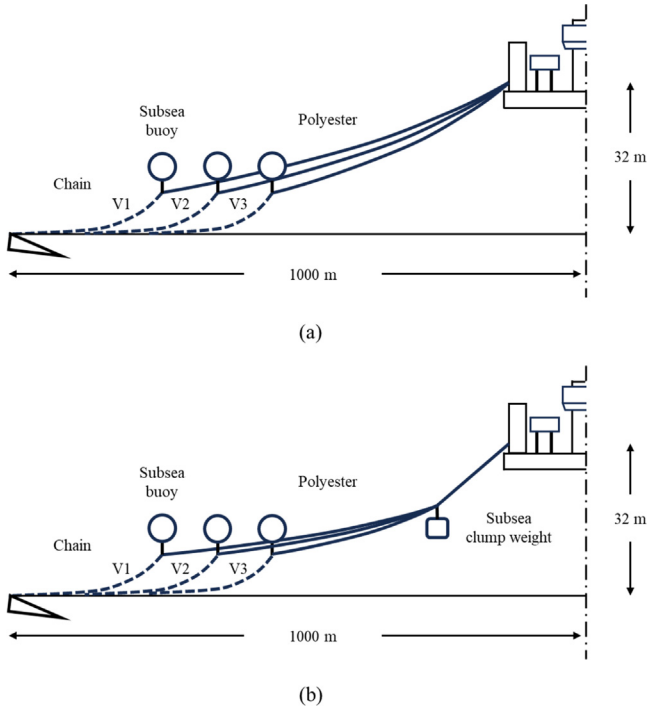

Fig. 11. Semi-taut variations (a) without clump weights and (b) with clump weights.

vestigated by attaching a clump weight to each polyester rope segment 100 m from the fairlead connection. All proposed semi-taut variations are depicted in Fig. 11 and the mooring system properties are given in Table 6. The complete design summary in Section 5.3 and Section 5.4 is shown in Fig. 12 for clarity.

6. Results and discussion

In this Section, validation of the STFC numerical model is performed and shown. Subsequently, the dynamic responses of STFC with different semi-taut variations are compared against those of a chain-catenary mooring system. The dynamic responses of STFC are presented in terms of platform motion responses, mooring line tensions and power absorption.

6.1. Numerical model validation

The response amplitude operators (RAOs) of the STFC numerical model used in this study are compared against that of the results as presented by Lee et al. [17]. Fig. 13 shows the comparison of RAOs for platform surge, platform pitch, flap no.2 rotation and torus heave. It is shown that within the considered wave periods, the RAOs of both models agree well with each other.

6.2. Mooring system restoring stiffnesses

Fig. 14 shows the restoring force-offset relationships for the investigated mooring designs in Table 6. The restoring stiffnesses of the baseline design in 200 m waters, “baseline (1084 m)” and the catenary-chain configuration, “chain-50 m (1084 m)” listed in Table 3 are also included for comparison. As the water depth decreases from 200 m to 50 m, the restoring stiffness of the catenary mooring system increases by approximately 480 % when the anchor radius remains unchanged. The increment is consistent with the trend predicted using Eq. (8). When the anchor radius is allowed to increase to 3000 m, the mooring restoring stiffness of a chain-catenary system can be reduced to a level similar to the semi-taut mooring systems.

As compared to the “chain-50 m (3000 m)” configuration, the semi-taut configurations have higher mooring restoring stiffnesses due to the small anchor radius (1000 m). It is observed that as the chain-to-rope ratio increases, the mooring system restoring stiffness increases. The addition of clump weights in the semi-taut variations results in reductions in the system restoring stiffness.

6.3. System natural periods

Numerical free decay tests are carried out to determine the natural periods of STFC’s supporting platform in the surge, heave, pitch and yaw degrees of freedom (DOFs). During the free decay tests, the wind turbine is put in parked condition with feathered blades while all WECs remain in operation. The resulting natural periods of the supporting platform with different mooring systems are shown in Fig. 15.

The natural periods for the platform pitch motions remain largely unaffected by the use of different mooring systems as they are dependent mainly on the hydrostatic stiffness and platform inertia. In the yaw DOF, the natural periods of the supporting platform with different mooring systems are close to each other due to similar horizontal pre-tensions. The platform heave natural periods are marginally affected by the vertical mooring force component. A higher departure angle at the fairleads and longer bottom chain length result in a higher vertical restoring force thereby increasing the mooring restoring stiffness in the heave direction. In terms of the platform’s surge DOF, lower mooring restoring stiffnesses result in “softer” systems and hence longer natural periods. All mooring configurations in 50 m waters result in surge natural periods in the region of 30–35 s, which are close to the pitch natural periods.

6.4. Motion responses

The response statistics of STFC platform motions are presented in terms of mean and standard deviation averaged across six random realizations for each EC. Figs. 16, 17 and 18 show the average statistics of surge, pitch, and yaw motions, respectively. All mooring configurations at a water depth of 50 m result in similar mean surge offsets in all ECs. The maximum mean surge offsets occur

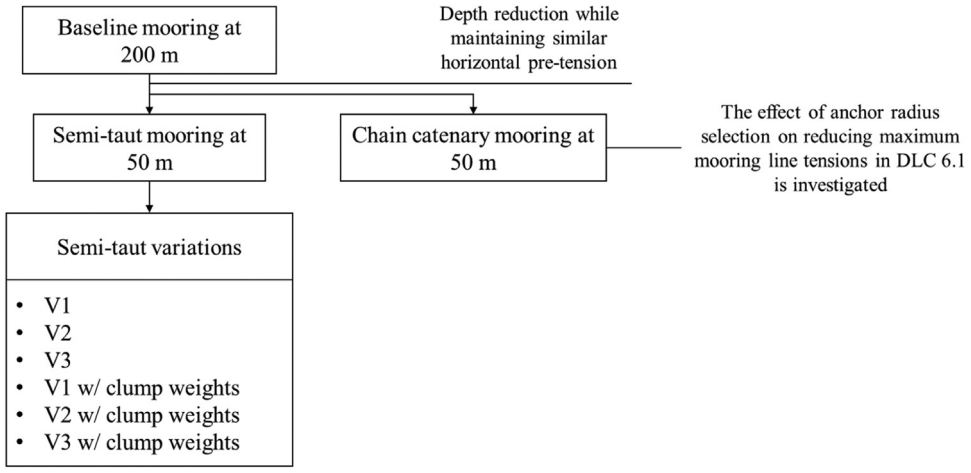

Fig. 12. Mooring design diagram.

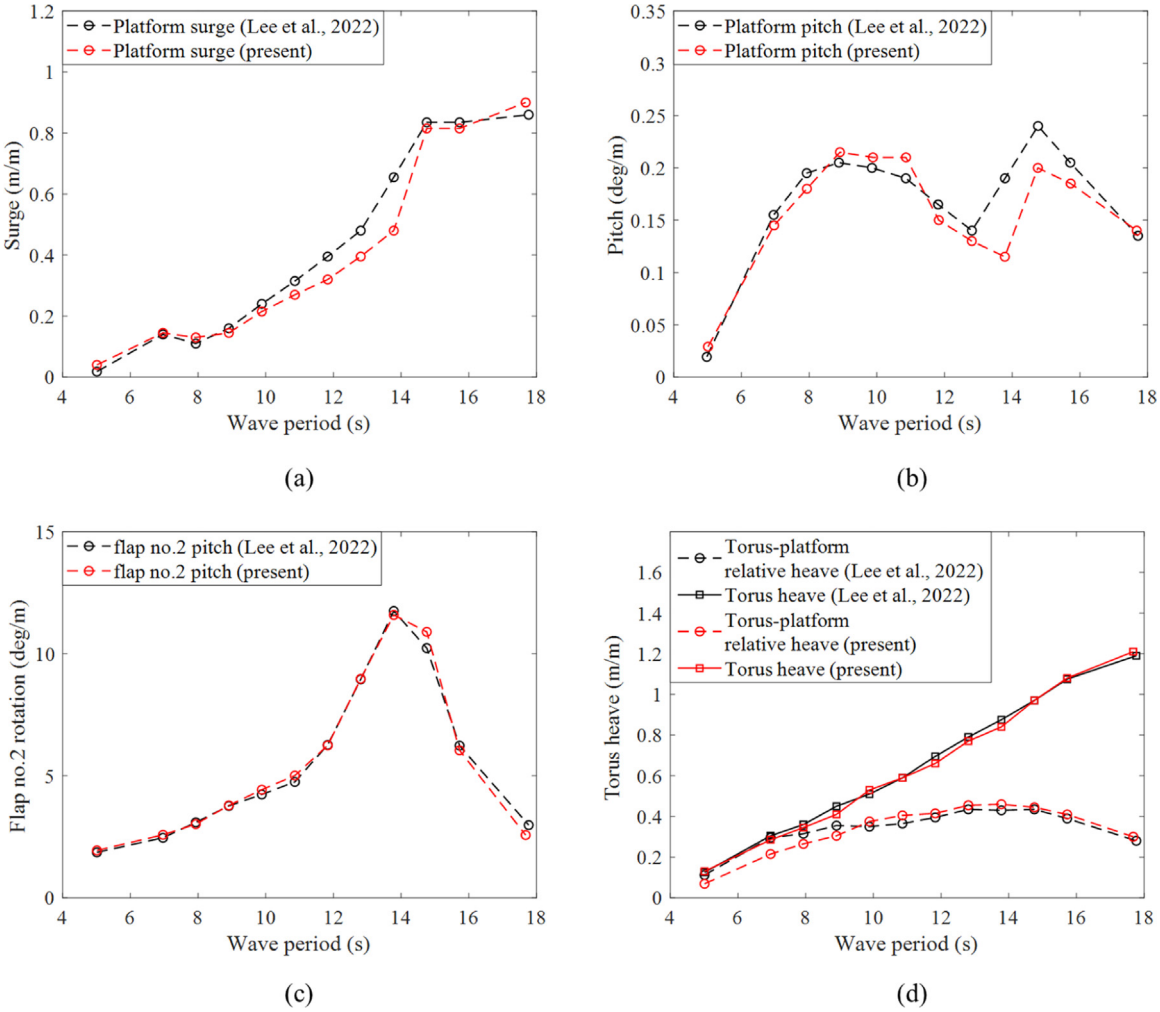

Fig. 13. RAO comparison for (a) platform surge, (b) platform pitch, (c) rotation of flap type WEC no.2 and (d) torus heave.

under EC2 with a hub height wind speed closer to the wind turbine's rated wind speed at 11.4 m/s. The "semitaut-V1clump" configuration results in the largest standard deviation in surge motion due to it being the "softest" system. As shown in Fig. 19, the high surge standard deviation is due to a significantly higher surge resonant response as compared to the other mooring configurations. The long bottom chain length of the "semitaut-V3" and "semitaut-V3clump" configurations yield the lowest surge responses among all configurations.

In terms of the pitch motion, the mooring designs do not have a significant effect on the mean pitch offset. However, the "chain-50m (3000 m)" configuration results in the lowest pitch standard deviation evident of the lowest pitch resonant response as shown in Fig. 20. The yaw restoring characteristics are not expected to

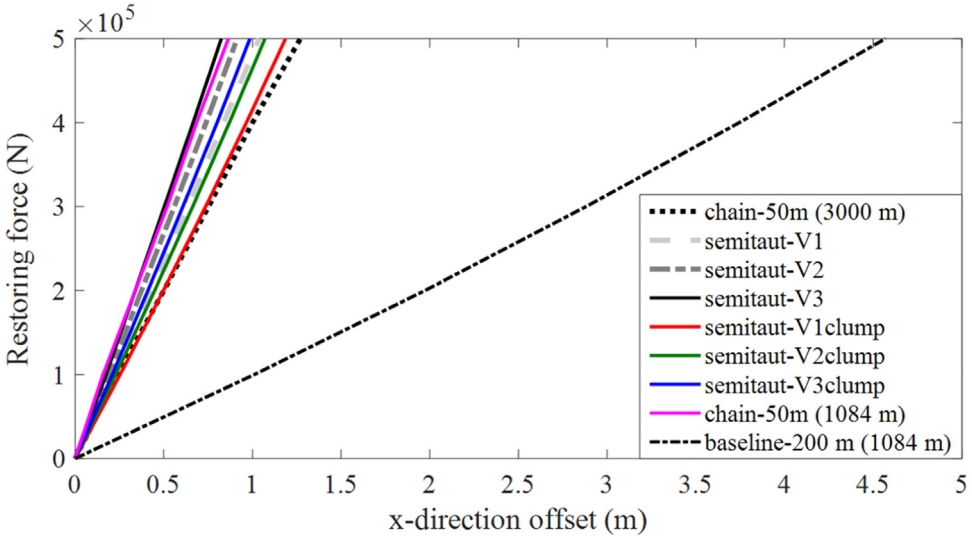

Fig. 14. Mooring system restoring forces for different mooring systems.

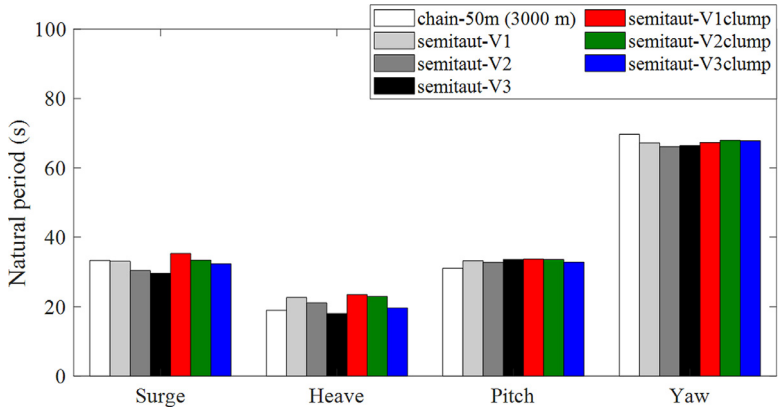

Fig. 15. System natural periods.

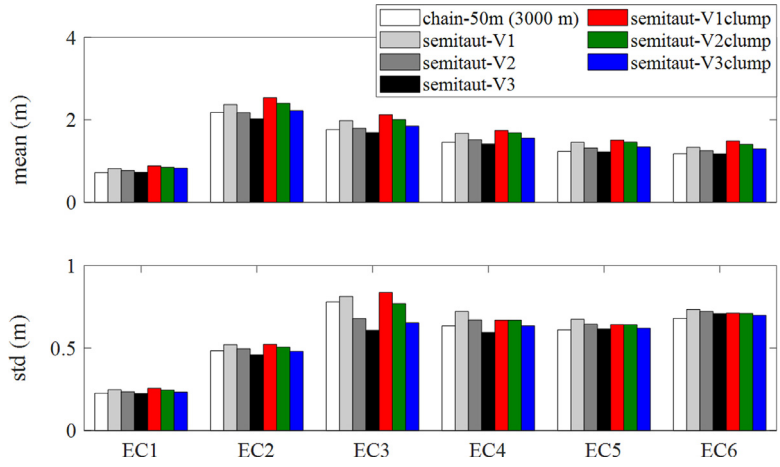

Fig. 16. 1-hour platform surge motion statistics in different ECs.

vary significantly across different mooring systems due to similar mooring pre-tensions. As shown in Fig. 21, the yaw resonant responses for all mooring configurations are in close agreement.

6.5. Mooring line tension

Fig. 22 shows the average statistics of the mooring line tension response for the windward mooring lines of different mooring configurations. The standard deviation of the tension response is the lowest for the "chain-50 m (3000 m)" configuration in all ECs due to the low surge resonant response as shown in Figs. 23. Despite having a significantly smaller anchor radius, the "semitaut-V1clump" configuration results in just a slight increase in surge resonant response as compared to "chain-50 m (3000 m)". This is due to a more compliant mooring restoring characteristics of the polyester rope. It is also observed that the addition of clump weights on the semi-taut systems reduces the wave-frequency responses of the mooring line tension. For the semi-taut systems,

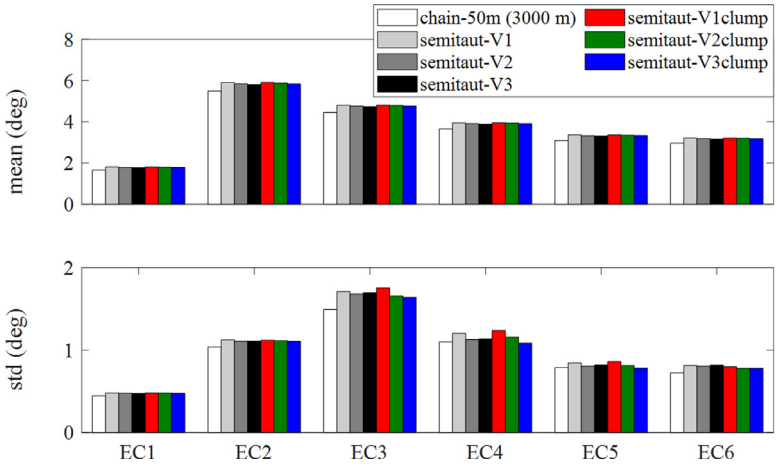

Fig. 17. 1-hour platform pitch motion statistics in different ECs.

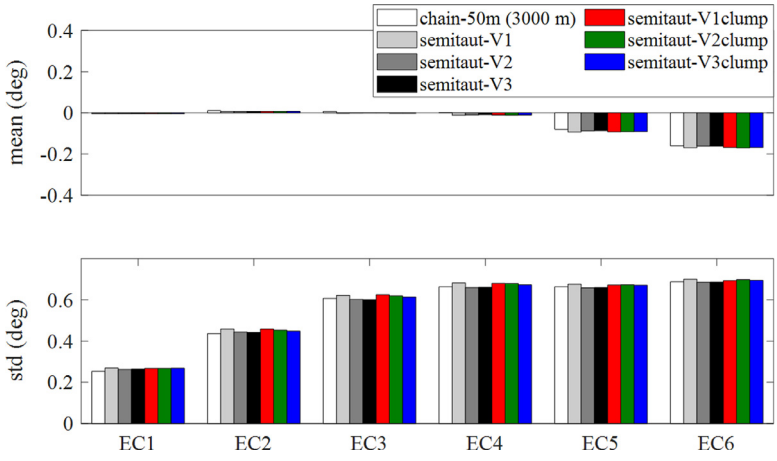

Fig. 18. 1-hour platform yaw motion statistics in different ECs.

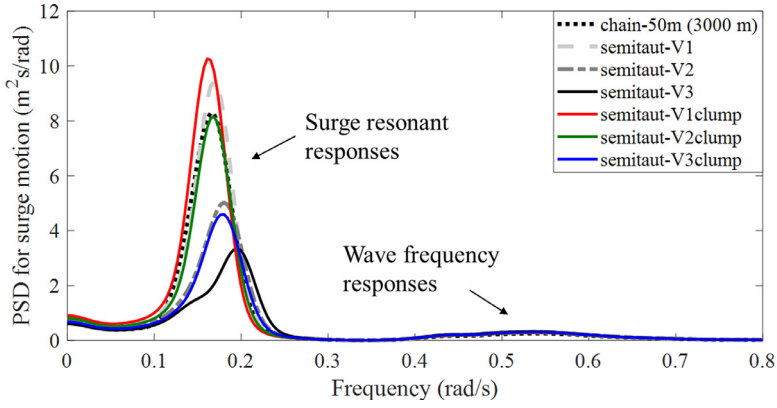

Fig. 19. PSD comparison of platform surge motions in EC3.

the tension standard deviations increase with increasing bottom chain lengths. With the longest bottom chain length of 578 m, the "semitaut-V3" configuration gives the highest tension response due to a combination of high surge resonant and wave-frequency responses.

In addition to the operational modes, the tension responses of STFC in the survival mode as described in Section 2.1 are investigated. Six random 3-hour simulations of STFC under DLC 6.1 are carried out. For each mooring configuration, the windward mooring line tension values are extrapolated using the mean up-crossing rate (MUR) method. Assume that high up-crossings are statistically independent events, the probability of occurrence can be estimated by,

$$F(y) = \exp\left[-\bar{\nu}^{+}(y)T\right] \tag{10}$$

where T is the period and $\bar{\nu}^{+}$ is the empirically measured mean up-crossing rate of response y given by [35],

$$\bar{\nu}^{+}(y) = q(y)\exp\left[-a\left(y-b\right)^{c}\right] \tag{11}$$

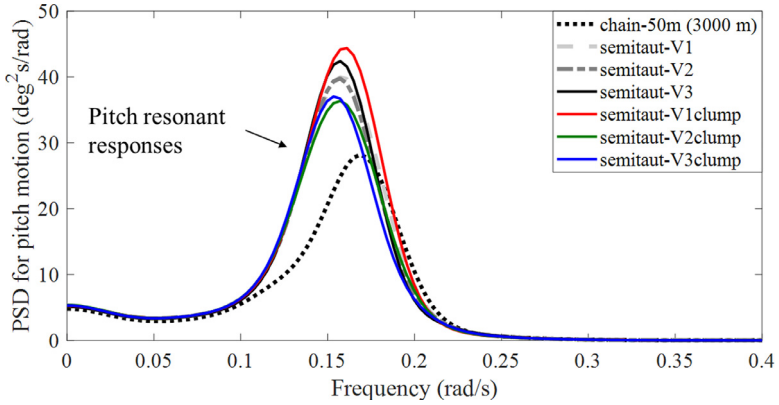

Fig. 20. PSD comparison of platform pitch motions in EC3.

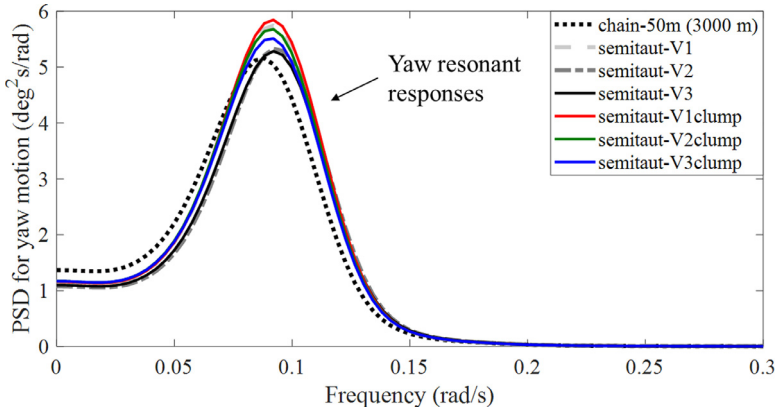

Fig. 21. PSD comparison of platform yaw motions in EC3.

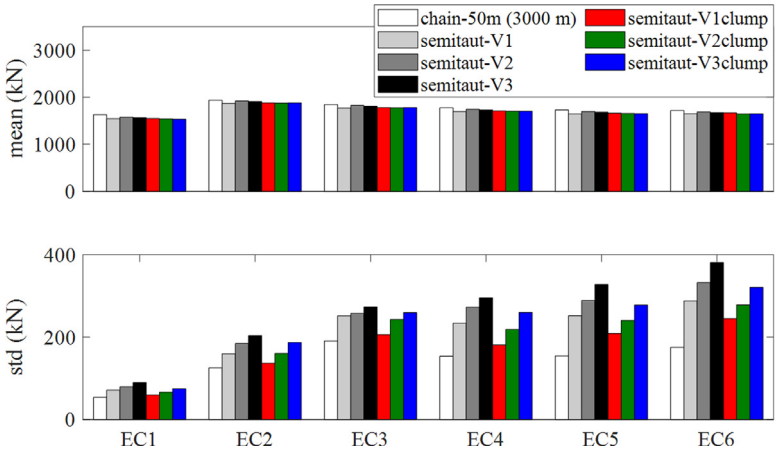

Fig. 22. 1-hour windward mooring line tension statistics in different ECs.

The fitting parameters a, b, c and d can be determined using a weighted optimization of the mean-square error function,

$$E = \sum_{j=1}^{n} w_j \left| \log \bar{\nu}^{+}(y_j) - \log q + -a(y_j - b)^c \right|^2 \quad (12)$$

where $w_j = [\log \mathrm{CI}^{+}(y_j) - \log \mathrm{CI}^{-}(y_j)]^{-1}$ is the weight factor that puts more emphasis of the fitting on the more reliably estimated values and $\mathrm{CI}^{\pm}$ is the 95 % confidence interval (CI) for $\bar{\nu}^{+}(y)$. Further details on the MUR method and the choice of w_j can be referred to Naess and Gaidai [36].

In this study, the 90 % fractile of mooring line tension maxima is used for comparative analysis. Table 7 shows the maximum tensions of the windward mooring lines for all mooring configurations. Although the "chain-50m (3000 m)" configuration exhibits the lowest standard deviations under operating environmental conditions, it leads to the highest maximum tension in DLC 6.1. Comparing the "semitaut-V1" and "semitaut-V3" configurations, the maximum mooring line tension increases by approximately 19 % with a 53 % increase in bottom chain length. Despite having a significantly smaller mooring footprint, all semi-taut mooring configurations result in lower maximum tensions than the "chain-50m (3000 m)" configuration.

From the perspective of maximum tension reduction, semitaut mooring configurations with clump weights achieve a modest reduction of approximately 1–2% in maximum tension com-

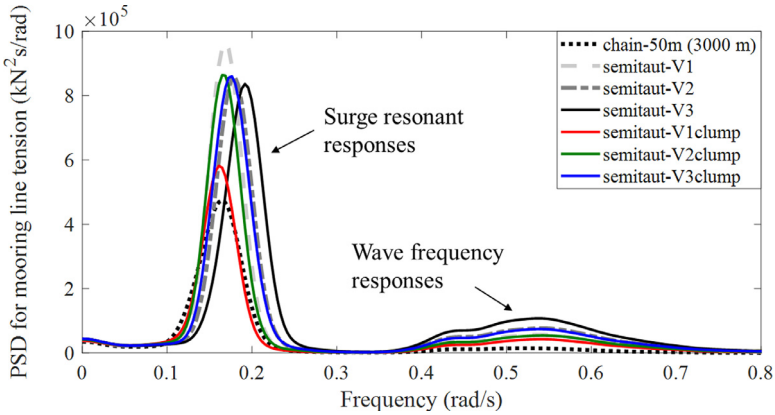

Fig. 23. PSD comparison of windward mooring line tensions in EC3.

Table 7
Maximum surge offsets and maximum windward mooring line tensions.

	Maximum surge offset (m)	Maximum tension (kN)	% MBS
chain-50 m (3000 m)	14.5	9911.9	83.07
semitaut-V1	15.2	7620.1	64.73
semitaut-V2	14.6	8297.0	70.48
semitaut-V3	14.1	9057.0	76.94
semitaut-V1clump	15.0	7529.4	63.96
semitaut-V2clump	15.0	8177.6	69.47
semitaut-V3clump	14.3	8940.7	75.95

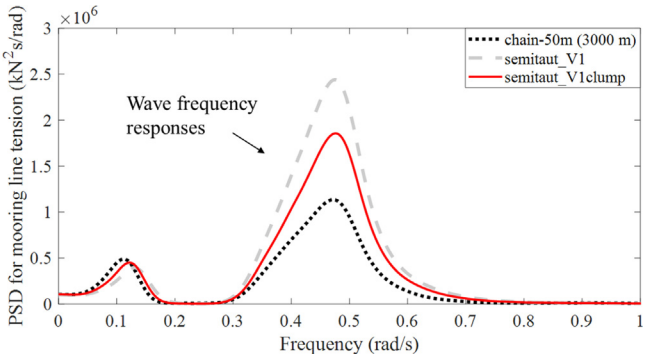

Fig. 24. PSD comparison for windward mooring line tensions in DLC 6.1.

pared to those without clump weights. Moreover, the inclusion of clump weights effectively reduces wave-frequency excitations. Fig. 24 shows the comparison of the PSD for windward mooring line tensions in DLC 6.1 for three selected mooring systems. The addition of clump weights to the "semitaut-V1" configuration results in an effective damping of the tension response in the wave excitation frequency range.

6.6. Power production

Figs. 25 and 26 show the power production of the wind turbine and the WECs, respectively. It is shown that the different mooring configurations do not result in significant changes in the power production of STFC. In the most severe operational sea state (EC6), the combined mean power production of the flap-type and torus WECs constitutes approximately 18 % of the total power output of the STFC.

6.7. Cost estimates

In this section, a basic cost analysis of the examined mooring designs is presented, concentrating on material, component, and installation expenses. In recent years, considerable effort has been put into investigating component and installation costs across different types of mooring systems ([37], Myhr et al., 2014, [4]). The cost analysis in this study draws upon data from the previously cited references. The material and component costs can be estimated given by,

Table 8
Cost of mooring line materials, components and installation.

		Price
Mooring line material	Steel chain	2.4525 €/kg
	Polyester rope	6.8670 €/kg
Mooring component	DEA	114,000 €/piece
	SA	512,500 €/piece
	Buoy	2 €/kg buoyancy
Installation		55,000 €/line

$$C = \left(\underbrace{C_l \times l \times m \times u}_{\text{rope material}} + \underbrace{C_c}_{\text{component}} \right) \tag{13}$$

where C_l is the material cost per unit weight, m is the mooring mass per unit length, l is the mooring line length, C_c is the cost of components and u is the mooring line utilization factor. DNV [38] stated that the utilisation factor of mooring lines can be calculated given by,

$$u = \frac{T_{pre}\gamma_{pre} + \left(T_{MPM} - T_{pre}\right)\gamma_{dyn}}{0.95 \times \text{MBS}} \tag{14}$$

where T_{pre} is the pre-tension, T_{MPM} is the most probable maximum (MPM) tension, γ_{pre} and γ_{dyn} are the safety factors which are 1.3 and 1.75, respectively. The cost of chain and polyester ropes in €/kg are based on the data provided by Xu et al. [4]. The cost the buoys is priced at 2 € per kg of net buoyancy [39]. The cost of each DEA and suction anchors (SA) are 114,000 € and 512,500 €, respectively with a unit installation cost of 55,000 € [37]. Despite using DEA, the installation cost of the chain-catenary system is assumed to be equivalent to the systems using SAs. The material and component costs are outlined in Table 8.

The cost analysis is performed for the mooring systems with the cost breakdown and mooring line utility factors for three selected mooring configurations being presented in Table 9. To maintain similar utility factors at a 50 m water depth, the cost of chain-catenary mooring is the highest due to the long chain length and high utilization factor. Compared to the "semitaut-V1" and "semitaut-V1clump" configurations, the combined material and installation costs of the "chain-50m (3000 m)" configuration are more than double, rendering it economically unattractive.

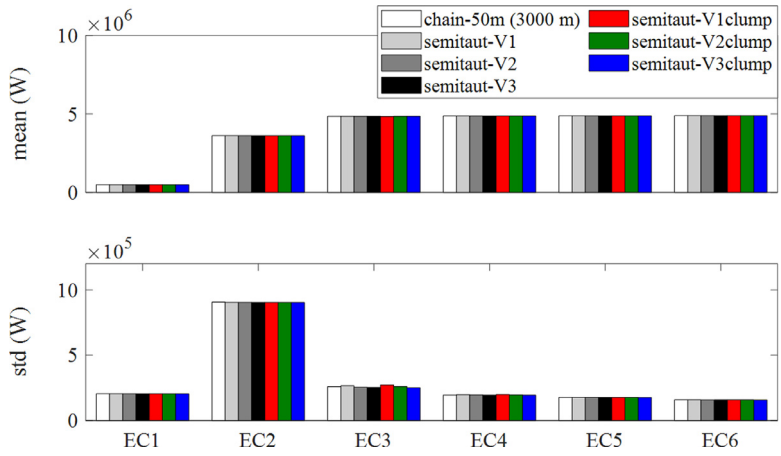

Fig. 25. 1-hour wind turbine power statistics in different ECs.

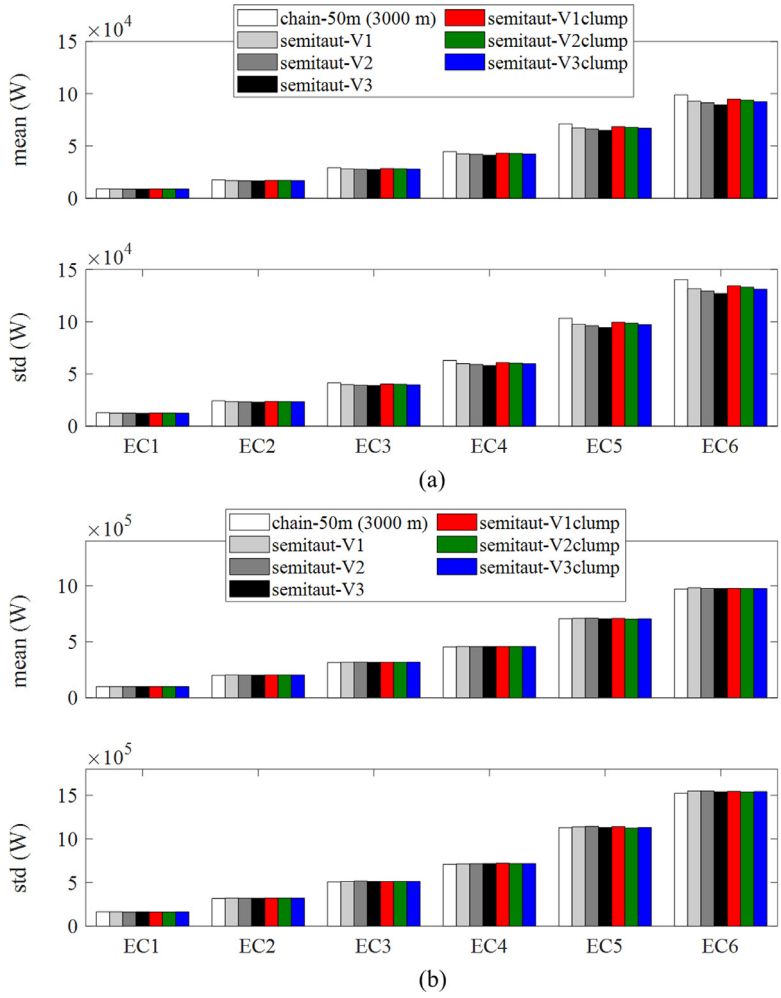

Fig. 26. 1-hour (a) flap type and (b) torus WECs absorbed power statistics in different ECs.

6.8. Design recommendations

Based on the findings in Sections 6.1 to 6.6, some design recommendations for the mooring system of STFC at intermediate water depth are provided in this section.

At intermediate water depths, the chain catenary systems excel in station keeping characteristics, attributed to the substantial chain weight that help maintain the mooring line geometry. However, the nonlinear restoring characteristics will incur sharp increases in dynamic mooring line tensions as more chains are being lifted-off the seabed. This problem can be alleviated by increasing the anchor radius which has an effect of reducing the mooring restoring stiffness and peak mooring line tension.

Another option for mooring solutions at intermediate waters is through the use of more compliant mooring system in the semi-taut configurations. The synthetic fibre rope segment of each moor-

Table 9
Cost estimation for three selected mooring systems.

	chain-50m (3000 m)	semitaut-V1	semitaut-V1clump	Unit
No. of mooring lines	3	3	3	(-)
Chain length	2958	377.9	377.9	(m)
Chain mass	370	370	370	(kg/m)
Polyester rope length	–	572.5	572.9	(m)
Polyester rope mass	–	26.5	26.5	(kg/m)
Utility factor	1.17	0.99	0.98	(-)
Clump	3 × 110	–	3 × 110	(k€)
Buoy	–	3 × 37.5	3 × 37.5	(k€)
Anchor	3 × 114	3 × 512.5	3 × 512.5	(k€)
Installation	3 × 55	3 × 55	3 × 55	(k€)
Total cost	10.26	3.15	3.46	(M€)

ing line has to be considerably longer than the water depth. Subsea buoys can be used to lift off the bottom chain segments and avoid any rope-to-seabed contact. While offering similar mooring restoring and tension response characteristics of the chain-catenary system, the semi-taut variations have a significantly smaller anchor radius. The semi-taut configurations result in mooring systems that are of significantly lower costs as compared to conventional chain catenary systems.

By adding clump weights to the mooring lines, the tension response near wave excitation frequencies can be effectively damped. This phenomenon is similar to the effect of tuned mass dampers commonly used to prevent resonance in high-rise buildings.

7. Conclusions

This study proposes and investigates different mooring systems for the STFC concept deployed at a water depth of 50 m. The global responses of STFC are simulated under operational and survival environmental conditions. The following conclusions can be drawn:

1. As compared to the semi-taut mooring systems, chain-catenary mooring systems require exceptionally large mooring footprints to keep the maximum tension well below the mooring line MBS.
2. With the use of semi-taut mooring systems, significantly smaller mooring footprints as compared to the chain-catenary mooring systems can be achieved.
3. In operating ECs, the “chain-50m (3000 m)” configuration provide similar mooring compliance as the semi-taut mooring systems while maintaining low tension standard deviations.
4. In extreme environmental condition, all semi-taut mooring systems outperform the “chain-50 m (3000 m)” configuration, resulting in significantly lower maximum mooring line tensions.
5. For the investigated semi-taut mooring systems, a longer segment of ground chain results in a higher mooring restoring stiffness and a larger mooring line tension standard deviation due to the increased wave-frequency response. One important consideration in the selection of ground chain length is the opportunity to move the platform surge natural frequency away from low-frequency excitation sources.
6. For the investigated semi-taut mooring systems, the wave-induced mooring line tension response is effectively reduced with the placement of a clump weight along each mooring line.

A basic cost analysis is performed. The present results shows that semi-taut mooring systems offer the possibility for significant cost reductions as compared to the chain-catenary system. Among the mooring systems studied, the “semitaut-V1clump” configuration demonstrates favourable tension responses and satisfactory motion characteristics, all while maintaining minimal mooring component and installation costs.

Declaration of competing interests

The authors declare that they have no known competing financial interests or personal relationships that could have appeared to influence the work reported in this paper.

Acknowledgements

The authors gratefully acknowledge the financial support through the Equinor Akademia program at the University of Stavanger. This study contributes to the ongoing work in IEA Task 49 Work Package 2.

References

[1] Renewables 2022 – Analysis and Forecast to 2027, Report, IEA PublicationsInternational Energy Agency, 2023.
[2] Floating Wind: Turning Ambition Into Action, Power and Renewables Report, DNV, 2023.
[3] T. Aderinto, H. Li, Ocean wave energy converters: status and challenges, Energies 11 (5) (2018) 1250.
[4] K. Xu, K. Larsen, Y. Shao, M. Zhang, Z. Gao, T. Moan, Design and comparative analysis of alternative mooring systems for floating wind turbines in shallow water with emphasis on ultimate limit state design, Ocean Eng 219 (2021) 108377.
[5] M. Francois, P. Davies, Fibre rope deep water mooring: a practical model for the analysis of polyester mooring systems, in: Proceedings of the Rio Oil and Gas Expo and Conference, Rio de Janeiro, Brazil, 2000.
[6] S.D. Weller, L. Johanning, P. Davies, S.J. Banfield, Synthetic mooring ropes for marine renewable energy applications, Renew. Ener 83 (2015) 1268–1278.
[7] A. Alexandre, Y. Percher, T. Choisnet, R.B. Urbano, R. Harries, Coupled analysis and numerical model validation for the 2MW Floatgen demonstrator project with Ideol Platform, in: Proceedings of the ASME 2018 1st International Offshore Wind Technical Conference, San Francisco, CA, USA, 2018.
[8] DNV-RP-E305: Design, Testing and Analysis of Offshore Fibre Ropes a, Recommended Practice, DNV, 2021.
[9] E. Falkenberg, V. Åhjem, L. Yang, Best practice for analysis of Polyester rope mooring systems, in: Proceedings of the Offshore Technology Conference, Houston, Texas, USA, 2017.
[10] S.H. Sørum, N. Fonseca, M. Kent, R.P. Faria, Modelling of synthetic fibre rope mooring for floating offshore wind turbines, J. Mar. Sci. Eng 11 (1) (2023) 193.
[11] S.H. Sørum, N. Fonseca, M. Kent, R.P. Faria, Assessment of nylon versus polyester ropes for mooring of floating wind turbines, Ocean Eng 278 (2023) 114339.
[12] D7.9 LCOE Analysis for Baseline Project Scenarios, Report, European Scalable Offshore Renewable Energy Source, 2022.
[13] L. Martinelli, P. Ruol, G. Cortellazzo, On mooring design of wave energy converters: the Seabreath application, Coast. Eng. Proceed 1 (33) (2012) structures.3.
[14] Flex2power, 2023, Official website, https://flex2power.com/, accessed September 2023.
[15] K.L. McTiernan, K.T. Sharman, Review of hybrid offshore wind and wave energy systems, J. Phy.: Conf. Series 1452 (2020) 012016.
[16] M.J. Legaz, D. Coronil, P. Mayorga, J. Fernández, Study of a hybrid renewable energy platform: W2Power, in: Proceedings of the ASME 37th International Conference on Ocean, Offshore and Arctic Engineering, Madrid, Spain, 2018.
[17] C.F. Lee, C. Tryfonidis, M.C. Ong, Power performance and response analysis of a semi-submersible wind turbine combined with flap-type and torus wave energy converters, J. Offshore Mech. Arctic Eng 145 (4) (2022) 042001.
[18] C. Luan, Z. Gao, T. Moan, Design and analysis of a braceless steel 5-MW semi–submersible wind turbine, in: Proceedings of the ASME 35th International Conference on Offshore Mechanics and Arctic Engineering, Busan, South Korea, 2016.

[19] J. Jonkman, S. Butterfield, W. Musial, G. Scott, Definition of a 5-MW Reference Wind Turbine for Offshore System Development (NREL/TP-500-38060), NREL, 2009.
[20] SINTEF Ocean, 2021a. RIFLEX 4.20.3 user guide.
[21] SINTEF Ocean, 2021b. SIMO 4.20.3 user guide.
[22] DNV, 2016, HydroD User Manual, DNV.
[23] J.F. Flory, V. Anjem, S.J. Banfield, A new method of testing for chang-in-length properties of large fiber-rope deepwater mooring, in: Proceedings of the Offshore Technology Conference, Houston, Texas, U.S.A, 2007.
[24] D.S. Rowley, S. Leite, What if scenario testing of synthetic fibre rope for deepwater mooring systems, in: Proceedings of the Offshore Technology Conference, Rio de Janeiro, Brazil, 2011.
[25] B.J. Jonkman, TurbSim User's guide: Version 1.50", Technical Report No. NREL/TP-500-46198, National Renewable Energy Laboratory, Golden, CO, 2009.
[26] K. Johannessen, T.S. Meling, S. Haver, Joint distribution for wind and waves in the northern North Sea, Int. J. Offshore Polar Eng 12 (2) (2002).
[27] Wind energy generation systems part 3-1: design requirements for fixed offshore wind turbines, 2019.
[28] M. Brommundt, L. Krause, K. Merz, M. Muskulus, Mooring system optimization for floating wind turbines using frequency domain analysis, Energy Procedia 24 (2012) 289–296.
[29] G. Benassai, A. Campanile, V. Piscopo, A. Scamardella, Mooring control of semi–submersible structures for wind turbines, Procedia Eng. 70 (2014) 132–141.
[30] A.C. Pillai, T.J. Gordelier, P.R. Thies, C. Dormenval, B. Wray, R. Parkinson, L. Johanning, Anchor loads for shallow water mooring of a 15 MW floating wind turbine — Part I: Chain catenary moorings for single and shared anchor scenarios, Ocean Eng. 266 (2022) 111816.
[31] O.M. Faltinsen, Sea Loads on Ships and Offshore Structures, Cambridge University Press, 1993.
[32] BRIDON BEKAERT, 2013, Advanced rope solutions for the offshore oil and gas exploration, construction and production industries, product catalogue, BRIDON BEKAERT.
[33] Ramnäs, Top Quality Mooring Products for Harsh offshore conditions, Ramnäs Bruk product catalogue, Ramnäs Offshore AB (2012).
[34] M. Tomren, Design and Numerical Analysis of Mooring Systems For Floating Wind Turbines – Comparison of Concepts for European Waters, Master's thesis, NTNU, Trondheim, 2022.
[35] A. Naess, O. Gaidai, P.S. Teigen, Extreme response prediction for nonlinear floating offshore structures by Monte Carlo simulation, Appl. Ocean Res 29 (4) (2007) 221–230.
[36] A. Naess, O. Gaidai, Estimation of extreme values from sampled time series, Struct. Saf 31 (2009) 325–334.
[37] C. Bjerkseter, A. Ågotnes, Levelised Costs of Energy for Offshore Floating Wind Turbine Concepts, Master's thesis, Norwegian University of Life Sciences, Ås, 2013.
[38] DNV-ST-0119: Floating Wind Turbine Structures b, Standard, DNV, 2021.
[39] Economic and Environmental Criteria and Assessment Methodologies For Moorings and Foundations, 2015 Report, DTOcean.